A Hardware-in-the-Loop Approach to Test Rotary Electromagnetic Shock Absorbers

IEEE Access
Multidisciplinary | Rapid Review | Open Access Journal

Received 22 April 2024, accepted 9 May 2024, date of publication 13 May 2024, date of current version 20 May 2024.

Digital Object Identifier 10.1109/ACCESS.2024.3400676

APPLIED RESEARCH

A Hardware-in-the-Loop Approach to Test Rotary Electromagnetic Shock Absorbers

MANFREDI TORNABENE[1], GENNARO SORRENTINO[1,2], RENATO GALLUZZI[3], (Senior Member, IEEE), ANDREA TONOLI[1,2], AND NICOLA AMATI[1,2]

[1]Department of Mechanical and Aerospace Engineering, Politecnico di Torino, 10129 Turin, Italy
[2]Center for Automotive Research and Sustainable Mobility, Politecnico di Torino, 10129 Turin, Italy
[3]School of Engineering and Sciences, Tecnológico de Monterrey, Mexico City 14380, Mexico

Corresponding author: Renato Galluzzi (renato.galluzzi@tec.mx)

This work was supported by Marelli Ride Dynamics in the context of a private research contract between the company and Politecnico di Torino.

ABSTRACT Electromagnetic shock absorbers are mechatronic actuators designed to improve ride comfort and road holding in ground vehicles by introducing variable active and damping forces in the suspension. This feature difficults their testing, as the characterization test bench must adapt to this variable load feature. Moreover, there is interest in testing them under realistic use scenarios. In this context, this work focuses on a hardware-in-the-loop implementation on a custom damper test bench to characterize rotary electromagnetic shock absorbers. First, the used test bench is presented and described. The model of the plant is obtained together with a quarter car model of the target vehicle. Test bench bandwidth and instability issues are discussed. Then, a model following compensation method is proposed and simulated. Finally, the resulting approach is used to control the testbed, where the quarter car model is used to produce a realistic load duty cycle in real time. Experiments highlight the tracking performance of the test rig and its robustness against load variations.

INDEX TERMS Active suspensions, dampers, hardware in the loop, model following, rotary regenerative shock absorbers, test bench.

I. INTRODUCTION

Modern vehicle dynamics research mainly focuses on the possibility of actively controlling the vehicle chassis to enhance its performance in many different regards. Controllable suspensions focus on the vertical degrees of freedom by introducing a control action to modulate the forces of the suspension assembly, i.e. spring and shock absorber. The automotive suspension as a mechatronic device has been studied extensively in recent years. Fischer and Isermann [1] proposed a classification of controllable suspensions according to their control range, bandwidth, and control variable. According to their proposal, *adaptive* and *semi-active* suspensions are essentially passive systems because they do not introduce mechanical energy to the vehicle. Thus, they work in the passive quadrants (II and IV) of the force-speed plane. Their technology is usually based on fluids with variable rheology [2], [3] or controllable hydraulic pressure loads [4], ensuring a fast damping control with very low power consumption. In contrast, *slow-active* and *full-active* suspensions can provide forces in all the four quadrants of operation. It is worth noting that the behavior of passive components, such as a spring and a damper, lies inside this plane. Hence, the additional action of an active device can be superimposed to these passive components and, ideally, it could fully replace them. Electromagnetic dampers can fall into the active damper category. They have a force/torque-controlled electric machine at their core, which can be paired with a proper transmission stage. As evidenced by several previous works [5], the intrinsic reversibility of electric machines enables the possibility of harvesting the vibrational energy coming from road irregularities when

The associate editor coordinating the review of this manuscript and approving it for publication was Guilin Yang.

operating in the passive quadrants. Numerous efforts have focused on different implementations of electromagnetic technologies for damping. Gysen et al. [6] discussed an example of regenerative linear electromagnetic shock absorbers. Galluzzi et al. focused specifically on rotary regenerative shock absorbers, both electro-hydrostatically actuated [7] and electromechanically actuated [8].

Rotary solutions are more difficult to implement in a suspension scheme due to the need for a rotary-to-linear conversion mechanism. Nevertheless, their increased force density when compared to linear motors justifies their application [9]. Particularly, the tested shock absorber in this work is an updated version of the system proposed by Galluzzi et al. [8] and it will be referred as rotary electromagnetic shock absorber (REmSA). When comparing this device to other controllable shock absorbers, including those that are electromagnetic, its main advantages are its elevated maximum efficiency ($\sim$ 80%), extended control bandwidth, and oil-free feature. Moreover, it opens the possibility of rethinking the overall suspension architecture, aiming for a lower center of gravity and a dome-free design. On the other hand, some challenges must be addressed, such as high power consumption during active operations, an additional non-negligible inertia between the two masses of the corner, gear meshing noise [10], and the absence of a fail-safe functionality in the absence of electrical power.

Damper characterization usually involves harmonic perturbations on the tested device. Typically, linear motion is applied, while reaction force is measured and logged. While this approach has become a typical practice for passive devices, it becomes a limited means of characterization for controllable devices, specifically active ones. Moreover, rotary devices require additional mechanical integration to convert linear displacements of the machine into crank rotation. More importantly, active devices are more sensitive to overheating due to temperature limits of electric machine components (windings and permanent magnets). Then, testing must pinpoint significant and realistic operating points without excessive cycling, which can damage the tested specimen. An innovative and specific testing approach for electromagnetic dampers is required.

Hardware-in-the-loop (HiL) techniques for vehicle suspensions imply to physically test the suspension or one of its components by means of a real-time vehicle simulation. This numerical representation is fed with the actuator force, as it supplies proper motion to the tested device. Previous research efforts have explored the idea of implementing HiL before. Misselhorn et al. [11] presented a possible setup for HiL suspension testing. Batterbee and Sims [12] were able to test a magnetorheological semi-active damper with controlled damping and sky-hook control strategy through HiL. Beliautsou et al. [13] enhanced HiL testing by interconnecting different test benches with vehicle subsystems, including one for active shock absorbers.

Another approach to test controllable suspensions in a laboratory setup is to physically reproduce one corner of the vehicle. As Lauwerys et al. [14] describes, a quarter car test rig vertically excites a wheel connected by means of the vehicle suspension to a cantilever mass reproducing the sprung mass. The main advantage of this method is the reproduction of the nonlinear behavior in suspension kinematics, as highlighted by the multibody modeling of the test bench presented by Sandu et al. [15]. Moreover, quarter car testbeds facilitate the testing campaign for nonlinear dampers since links can be added to the suspension. For example, Yu et al. [16], [17] tested an electromechanical active shock absorber linked to a double-wishbone suspension. Additionally, quarter car test rigs can be reproduced physically through simplified layouts with two bulk masses, i.e the wheel body and the wheel, as described by Taskin et al. [18].

In this context, both HiL and quarter-car test rigs offer important flexibility and realism to active damper characterization. However, the recreation of a quarter car setup is usually more costly, as it requires more parts, larger space, and more powerful actuators to reproduce the road unevenness. Although the choice of HiL would seem straightforward, it introduces important limitations related to the dynamics of sensors and actuators. The overall system bandwidth will be dictated by the delays that these elements introduce. Furthermore, the dynamic behavior and stability of the system will be determined by the interaction of these components with the tested specimen. Consequently, test results will be inevitably affected by these interactions. Different compensation techniques can be explored to limit these issues. Hashemi et al. [19] proposed a polynomial compensation technique to take into account actuator and sensor time delays in a HiL jet engine fuel control unit. Chen and Ricles [20] experimentally evaluated three different compensation methods based on equivalent discrete transfer function. The latter can be taken as state of the art for servo-hydraulically actuated real-time test benches.

This research work proposes a HiL approach to test REmSA devices. The starting point is the electro-hydrostatic test rig for characterizing electromagnetic shock absorbers discussed by Tonoli et al. [21]. To improve the capabilities of this testbed, two key upgrades were executed: (i) the installation of a mechanical interface to test REmSA devices, and (ii) the implementation of a model following compensation method to guarantee stability and sufficient actuation bandwidth. Furthermore, the proposed methodology demonstrates suitable adaptability to a wide range of load variations, which is a typical feature of controllable suspensions. Hence, this paper focuses on the assessment of the test bench tracking performance when included in a HiL system and disregarding the behavior of the device being characterized.

This paper is organized as follows. First, Section II describes the electro-hydrostatic test bench and the prototype,

with focus on their dynamic models. Then, simulation results about the HiL model are discussed, with particular attention to the actuation bandwidth and the stability issues when the test bench model is integrated with a numerical quarter car model. A model following method is implemented to stabilize the system and yield sufficient actuation bandwidth. In Section III, an experimental campaign aims to physically evaluate the HiL performance of a REmSA and asses the compensation method robustness to different loads. Finally, Section IV concludes the work.

II. METHOD

This section outlines the approach behind the HiL tests for a REmSA. After presenting the test bench layout, the system is modeled to reproduce the test bench dynamics in virtual environment. Then, the designed compensation method is formulated and tested numerically on the plant model.

A. TEST BENCH LAYOUT

The electro-hydrostatic test rig considered in this study is shown in Fig. 1. Its goal is to apply alternating or irregular displacement profiles to the REmSA. To this end, the output shaft of the REmSA is connected to a hydraulic actuator by means of a lever of length $l_r = 115\,\text{mm}$. The actuator consists of a cylinder with a double-acting, through-rod piston with area $A_p = 6.4\,\text{cm}^2$. A positive-displacement pump supplies hydraulic power to the piston, since each chamber of the cylinder is directly connected to a port of the pump (Parker^{TM} MGG20030 with displacement $D_p = 11.4\,\text{cm}^3/\text{rev}$). The pressure of the lines is measured through two membrane sensors (Gefran^{TM} TK). A fluid pre-charge pump is connected to one of the two lines to set a static pressure value of 18 bar before starting the whole testing procedure. This setpoint is needed to avoid cavitation in the hydraulic circuit while driving an elevated pressure delta. The shaft of the pump is mechanically coupled to a driving motor (Kollmorgen^{TM} DBL51700 brushless PM motor) by means of a bellows expansion joint. This actuation layout is intrinsically bidirectional, i.e. it can yield alternate motion. It is also intrinsically reversible, as it can absorb or exert mechanical power to the tested load. A dedicated inverter unit (Kollmorgen^{TM} Servostar S748) is devoted to control the driving motor. The hydraulic piston is equipped with a magnetostrictive position transducer (Gefran^{TM} RK2) to measure its stroke. A load cell (Gefran^{TM} TU K5C) is installed between the piston head and the load lever tip to measure the exchanged force. The generated load signal is then conditioned by means of a MGCplus^{TM} Data Acquisition system and provided as analog output. All these signals are fed into a dSpace^{TM} MicroLabBox, which also serves as a control unit for rapid prototyping. The REmSA prototype is controlled by means of a dedicated electronic control unit, which is supplied by a custom 48-V lithium ion battery pack. The control stages of the driving motor, the REmSA, and the battery pack are interfaced with the dSpace^{TM} MicroLabBox (master node) using the Controller Area Network (CAN) protocol. In turn, the dSpace^{TM} MicroLabBox is connected to a PC, which serves as a human-machine interface.

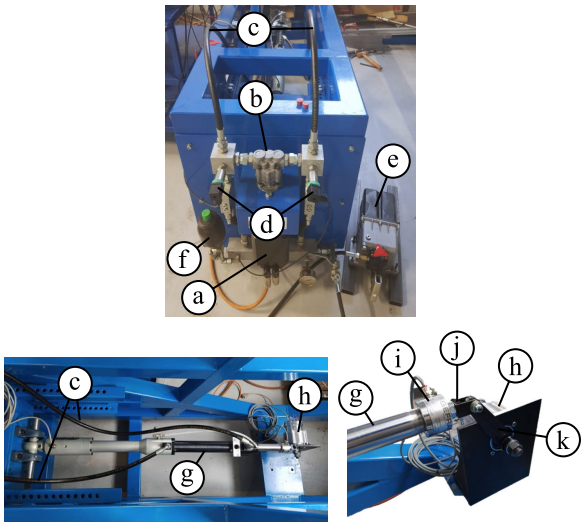

FIGURE 1. Test bench layout: (a) Driving motor, (b) hydraulic pump, (c) hydraulic lines, (d) pressure sensors, (e) pre-charge pump, (f) accumulator, (g) hydraulic actuator, (h) rotary electromagnetic shock absorber, (i) load cell, (j) ball joint, (k) lever.

B. TEST BENCH MODEL

To understand the dynamic behavior of the testbed and the load, its numerical model is developed according to the system shown in Fig. 2. The test bench actuator relies on a torque-controlled electric motor, which is represented as an ideal torque source T_{in}. This input drives the hydraulic pump through a rigidly coupled shaft. The inertia of the rotating parts of both the motor and the pump is lumped into J_θ. The viscous damping coefficient c_θ represents the mechanical losses in the rotary domain. The hydraulic pump acts as an ideal transformer by means of its volumetric displacement D_p. Its ports are connected to the hydraulic cylinder with two flexible lines. The fluid compliant behavior is lumped into hydraulic stiffness (k_h) and damping (c_h) terms. The piston inside the hydraulic cylinder transforms hydraulic variables into mechanical ones through the cross sectional area A_p. It has a mass m_p and damping coefficient c_p. This latter term represents the friction between the piston gasket seals and the cylinder walls. The rod attached to the piston is coupled to a lever of length l_r. In turn, the opposite end of this lever is attached to the shaft of the REmSA. This device has a gear multiplier, represented by a transmission ratio τ_r. The output of this gearbox is connected to an equivalent inertia J_{eq}, which lumps all the rotating elements inside the REmSA. Mechanical losses are described by a viscous damping coefficient c_{eq}. Finally, the electric

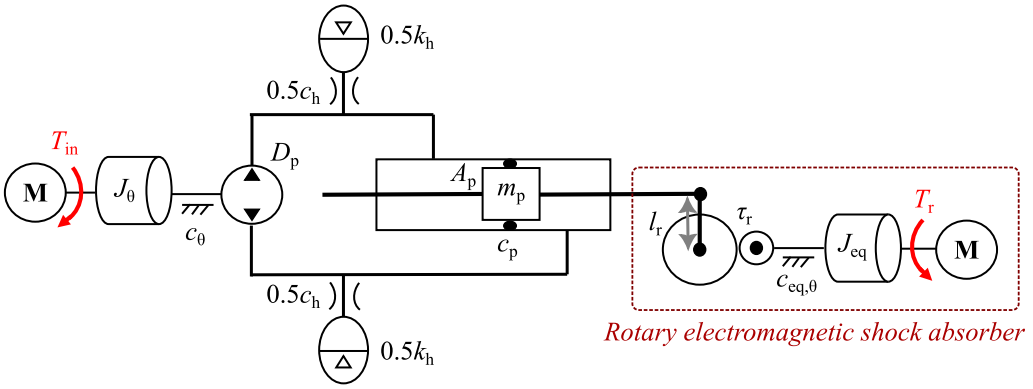

FIGURE 2. Lumped-parameter model of the test bench equipped with a rotary electromagnetic shock absorber.

machine of the REmSA is also represented as a torque source T_r.

Following this model description, a differential equation set can be established with three states:

$$\dot{\omega}_m = J_\theta^{-1}\left[-\left(c_\theta + D_p^2 c_h\right)\omega_m - D_p p_h + D_p A_p c_h v_p + T_{in}\right] \tag{1}$$

$$\dot{p}_h = D_p k_h \omega_m - A_p k_h v_p \tag{2}$$

$$\dot{v}_p = \left(m_p + \frac{J_{eq}}{\tau_r^2 l_r^2}\right)^{-1}\left[D_p A_p c_h \omega_m + A_p p_h - \ldots \right.$$
$$\left. \ldots - \left(A_p^2 c_h + c_p + \frac{c_{eq}}{\tau_r^2 l_r^2}\right) v_p + \frac{T_r}{\tau_r l_r}\right] \tag{3}$$

where ω_m represents the angular speed of the motor-pump unit, p_h is the pressure acting on the circuit hydraulic stiffness, and v_p is the piston speed. Relevant parameters of this model are reported in Appendix A.

C. HARDWARE-IN-THE-LOOP MODEL

The test bench model described in Section II-B requires a control method to characterize the REmSA device under testing. Furthermore, being an active device, the REmSA itself needs coordinated control efforts according to the dynamics of the testbed. This synchronized regulation comes from a numerical model that describes (i) the suspension displacement imposed by the vehicle, and (ii) the force response exerted by the shock absorber. In this case, realistic vehicle dynamics are obtained in real time through a quarter car model, as seen in Fig. 3. This two-degree-of-freedom model describes the vertical dynamics of the chassis (sprung mass m_s, displacement z_s) and the wheel assembly (unsprung mass m_u, displacement z_u). The suspension assembly interconnects the chassis and the wheel by means of a passive damping c_s, a spring stiffness k_s, and an actuator with input force F_p. The tire is modeled through stiffness and damping elements k_u and c_u, respectively. The bottom end of the tire is subject to an irregular road displacement z_{road}.

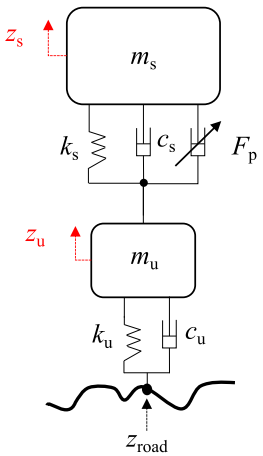

FIGURE 3. Quarter car model equipped with a controllable shock absorber.

The quarter car model is governed by two differential equations:

$$m_s \ddot{z}_s + c_s(\dot{z}_s - \dot{z}_u) + k_s(z_s - z_u) - F_p = 0 \tag{4}$$

$$m_u \ddot{z}_{us} + c_u(\dot{z}_u - \dot{z}_{road}) + k_u(z_u - z_{road}) + \ldots$$
$$\ldots + c_s(\dot{z}_u - \dot{z}_s) + k_s(z_u - z_s) + F_p = 0 \tag{5}$$

This mechanical system leads to a dynamic response governed by two natural frequencies [22]:

$$f_s = \frac{1}{2\pi}\sqrt{\frac{\left(k_s^{-1} + k_u^{-1}\right)^{-1}}{m_s}} = 1.13\,\text{Hz} \tag{6}$$

$$f_u = \frac{1}{2\pi}\sqrt{\frac{k_s + k_u}{m_u}} = 12.5\,\text{Hz} \tag{7}$$

which belong to the sprung and unsprung masses, respectively.

The integration of the plant, the quarter car and the controllers in a HiL model requires the definition of key variables. The speed of the actuator piston is directly related

to the angular speed of the REmSA motor

$$\omega_r = \frac{v_p}{\tau_r l_r} \tag{8}$$

and in turn, the electromagnetic torque provided by the REmSA motor is given by

$$T_r = K_r i_r = -c_{em,\theta}\omega_r \tag{9}$$

where K_r is the motor torque constant, i_r is its winding current, and $c_{em,\theta}$ is a rotary electromagnetic damping coefficient. Note that T_r follows the active sign convention and can be determined by a specific control strategy, such as sky-hook / ground-hook [23], linear quadratic regulator (LQR) [24] or H_∞ [25]. In this work, to simplify the analysis, T_r is computed as a viscous damping contribution. This target REmSA torque is achieved through a field-oriented control on the winding current i_r, which is the control variable of the REmSA.

When analyzing the behavior of the REmSA, it is important to quantify the force exchanged with the piston, which constitutes a measurable response of the actuator. This force is used for interaction with the quarter car model, as it represents the active contribution of the actuator. In a real vehicle setup, this will be the force exerted to the suspension assembly, which lumps the electromagnetic torque of the REmSA together with inertial (J_{eq}) and viscous damping ($c_{eq,\theta}$) contributions.

$$F_p = -\underbrace{\frac{c_{em,\theta}}{\tau_r^2 l_r^2}}_{c_{em}} v_p - \underbrace{\frac{c_{eq,\theta}}{\tau_r^2 l_r^2}}_{c_{eq}} v_p - \underbrace{\frac{J_{eq}}{\tau_r^2 l_r^2}}_{m_{eq}} \dot{v}_p \tag{10}$$

Note that in the linear domain, mass m_{eq} and damping terms c_{em}, c_{eq} appear. Coefficients m_{eq} and c_{eq} are usually undesirable. Although they can be attenuated through design guidelines, their presence is unavoidable.

The test bench motor-pump unit is controlled through a proportional-integral-derivative (PID) control to guarantee tracking on the angular displacement of the lever

$$\theta_l = \frac{1}{l_r}\int v_p dt \tag{11}$$

whose reference depends on the shock absorber stroke:

$$\theta_{l,ref} = \frac{1}{l_r}(z_s - z_u) \tag{12}$$

The command of this position control is the input motor current i_{in}, which yields the input torque

$$T_{in} = K_{in} i_{in} \tag{13}$$

Finally, the road profile z_{road} for the quarter car model is computed following the ISO 8608 standards [26], as suggested by Zuo and Zhang [5]. Imposing a constant longitudinal speed of the vehicle v_{car} and a road roughness coefficient G_r, the road displacement can be computed by filtering a unit-intensity white noise signal with the following first-order low pass filter, expressed in the Laplace domain:

$$G_{road}(s) = \frac{2\pi\sqrt{G_r v_{car}}}{s + \omega_0} \tag{14}$$

Following the described interactions among subsystems, the complete HiL scheme is illustrated in Fig. 4. Model and control parameters of the HiL scheme are also included in Appendices B and C.

D. COMPENSATION STRATEGY

Previous experiments on other shock absorbers have evidenced the limited frequency bandwidth of the test rig. The hydraulic nature of its transmission limits the bandwidth frequencies it can attain, especially when compared to an electro-mechanical test rig, which possesses an intrinsically stiffer transmission. Likewise, the maximum force is bounded by the ratings of the motor-pump unit. Furthermore, when working with active devices, their interaction with the testbed leads to phase delays, eventually yielding instability. Thus, a stabilization strategy is mandatory to enable proper tests.

First, the numerical reproduction of this instability is necessary. The closed-loop bandwidth of the testbed is evaluated by calculating the frequency response function of the position-controlled plant model when the REmSA damping is null ($\theta_l/\theta_{l,ref}$, $c_{em} = 0$). This first transfer function neglects the quarter car model block. The resulting frequency response function is shown in Fig. 5 (yellow line). It is characterized by a resonant peak at 15 Hz and subsequent attenuation.

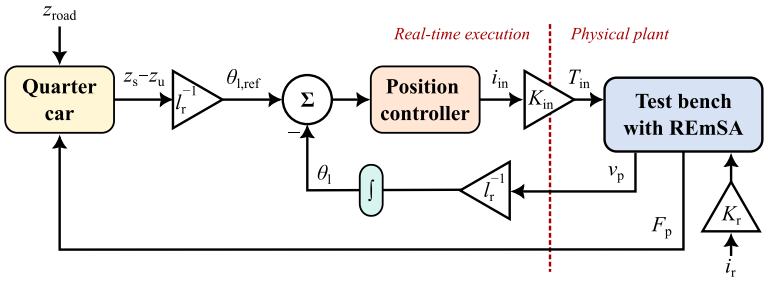

FIGURE 4. Hardware-in-the-loop scheme involving a quarter car model and position controller in real-time execution with the physical test bench plant. A rotary electromagnetic shock absorber (REmSA) is installed in the testbed.

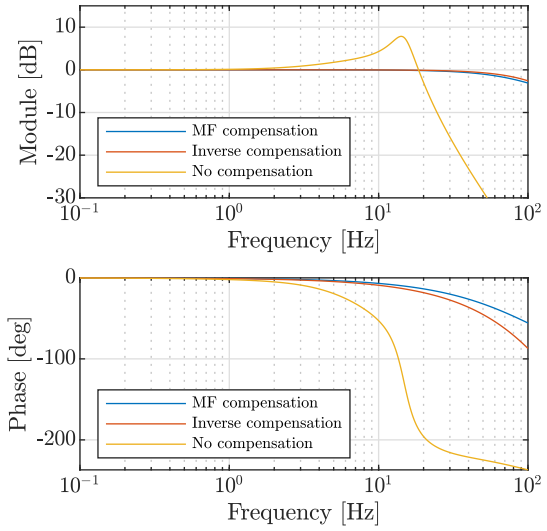

FIGURE 5. Frequency response of the closed-loop transfer function of the test bench ($\theta_l/\theta_{l,ref}$). Comparison between inverse compensation method, model-following method, and without compensation. All tests were executed with null REmSA damping.

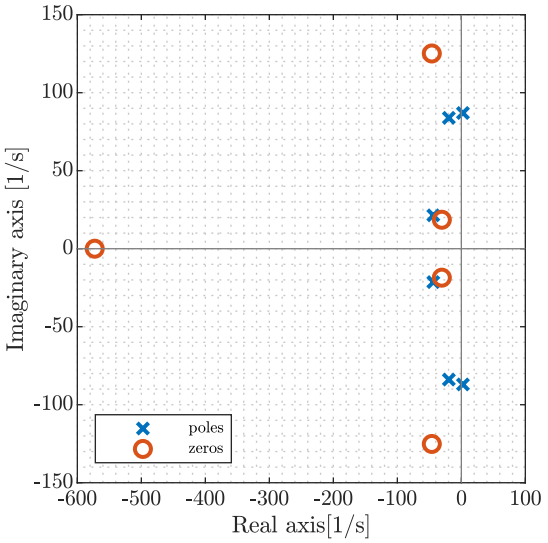

FIGURE 6. Root locus of the full HiL model transfer function z_s/z_{road}. Two complex conjugate poles with positive real parts lead to instability at a frequency close to the unsprung mass resonance.

The transfer function of the whole HiL model is then calculated to understand the dynamic response of the sprung mass vertical displacement with respect to the input road profile (z_s/z_{road}, $c_{em} = 0$). The root locus of this transfer function (Fig. 6) provides two complex conjugate poles with positive real parts that numerically prove the experienced instability of the actual test rig in HiL configuration. The natural frequency of these poles is 12.6 Hz, which is close to the unsprung mass natural frequency.

Moreover, the natural frequency of the unsprung mass is comparable to the test bench bandwidth ($\theta_l/\theta_{l,ref}$), which is slightly above 15 Hz. This implies that the test rig is unable to control unsprung mass dynamics. To mitigate the instability and increase the test bench bandwidth, a specific control strategy must be applied.

To stabilize the system, model following (MF) is applied through feedforward. This technique has been deeply studied by various researchers in many different applications. The main purpose of MF is to aid the plant output to track a reference model. This technique has been proposed in literature with implementations in different engineering solutions [27], [28]. In this work, MF imposes a dynamic behavior with larger bandwidth to the test bench.

Considering the scheme in Fig. 7, a transfer function G_p reproduces the dynamic behavior of the plant in open loop, i.e. output lever angle versus input current:

$$G_p(s) = \frac{\theta_l(s)}{i_{in}(s)} = \frac{k_1(s+z_1)}{s(s+p_1)(s+p_2)(s^2+a_1s+a_2)} \quad (15)$$

and its inverse is used as a feedforward action. The transfer function G_p^{-1} requires desirable inputs, which are produced by means of the transfer function G_d. This function is numerically implemented with a Bessel filter of order $n_{des} = 4$ and a cut-off frequency $f_{cut} = 500$ Hz, which yields a maximally linear phase response. In this case, the filter order has been imposed to obtain a causal implementation of G_d/G_p.

$$G_d(s) = \frac{k_2}{(s+p_3)(s+p_4)(s^2+a_3s+a_4)} \quad (16)$$

Note that in the MF approach, G_d is also used to define the reference angle signal. Parameters for (15) and (16) are reported in Appendix D.

The developed numerical models are used to evaluate the plant frequency response. The resulting Bode diagrams are shown in Fig. 5. As previously stated, the test bench model without compensation starts the attenuation process after the peak resonance at 15 Hz. The MF compensation, instead, flattens the resonant peak and improves the available frequency bandwidth of the bench by shifting the heavy attenuation of the bench above 100 Hz, hence covering the entire bandwidth of interest in the quarter car model. Moreover, the MF strategy offers slightly improved performance when compared to inverse compensation [19], [20], [29]. Unlike MF, the inverse compensation does not apply a feedforward action. Referring to the MF diagram in Fig. 7, the transfer function G_p^{-1} is removed, and the transfer function G_d is replaced by the inverse of the closed-loop model ($\theta_{l,ref}/\theta_l$). Considering the plot in Fig. 5, the performance offered by the two compensation strategies is comparable, especially in the frequency range of interest. However, despite the similarity in terms of performance, the MF method is preferred for its definition. Its feedforward contribution G_p^{-1} does not depend on the controller parameters since the reference plant model G_p is referred to the input current i_{in} provided directly by the controller. The inverse method, instead, is based on a closed loop model function referred to the reference angle $\theta_{l,ref}$, hence including the controller

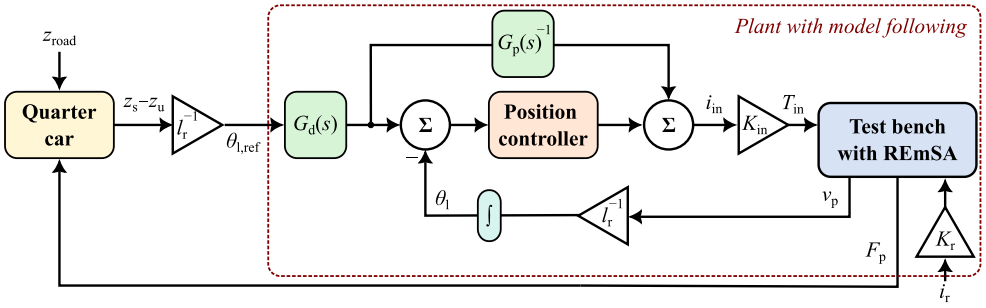

FIGURE 7. Model-following compensation method applied to the HiL model. A desired closed-loop transfer function G_d is used to provide input angular reference. Feedforward action must consider the inverse open-loop transfer function of the plant G_p^{-1}.

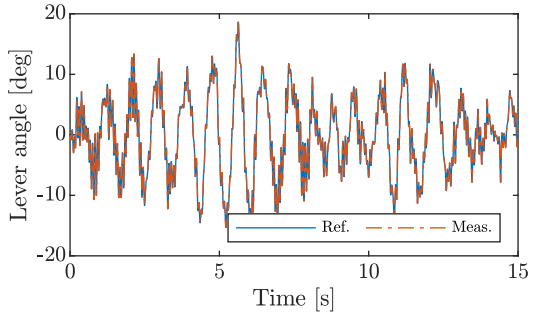

(a) $c_{em} = 0$

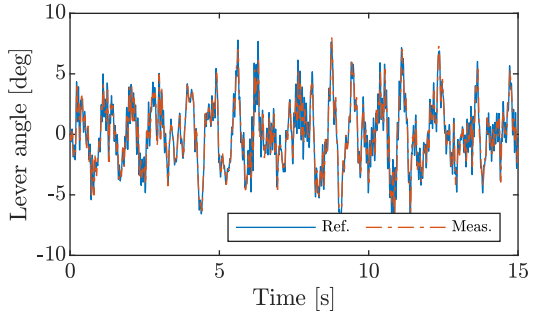

(b) $c_{em} = 1.5\,\text{kNs/m}$

FIGURE 8. Numerical tracking performance of the full HiL model with (a) null REmSA damping and (b) 1.5 kNs/m of REmSA damping. The quarter car model travels at 70 km/h on a ISO-B road profile.

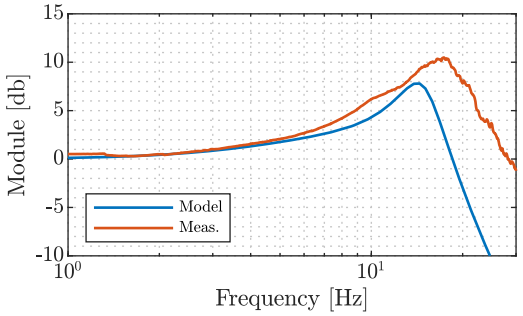

FIGURE 9. Test bench without compensation ($\theta_l/\theta_{l,ref}$): numerical and experimental frequency response functions with null REmSA damping. The experimental response is obtained with a reference angle sine sweep of 0.5 deg of amplitude and a frequency between 1 and 30 Hz.

inside its definition. Consequently, to freely choose the plant control type without affecting the compensation strategy, the MF method is preferred.

Once that the plant has been enhanced through MF, a verification is performed by interfacing it to the quarter car model. Simulations are performed with an ISO-B input road profile and a vehicle speed of 70 km/h. Responses with two REmSA damping coefficients were tested: null damping and 1.5 kNs/m. It is worth noting that MF compensation is tuned for the null damping case, which is the most unstable condition due to the low amount of damping in the system. This test is fundamental to understand the sensitivity of the MF approach to plant parametric variations. Angle tracking numerical results can be observed in Fig. 8 for both damping values. The angle tracking with null damping imposed by the REmSA model provides almost ideal results. Conversely, the system with 1.5 kNs/m of damping exhibits larger discrepancies between angle and reference. The performance of both cases can be quantified through the fit ratio

$$g = \left(1 - \frac{||\theta_{ref} - \theta_{meas}||}{||\theta_{ref} - \text{mean}(\theta_{ref})||}\right) \cdot 100\% \qquad (17)$$

where $g = 100\%$ indicates a perfect tracking. Thus, the null-damping simulation achieves $g = 95.5\%$, whereas the case where $c_{em} = 1.5\,\text{kNs/m}$ leads to a lower but acceptable $g = 75.2\%$. Thus, the effectiveness of the applied MF method through simulations provides a strong and solid starting point to set up an experimental HiL layout to test the strategy.

III. EXPERIMENTAL VALIDATION

In this section, the experimental campaign is presented with the aim of validating the HiL approach previously described. The starting point is the experimental characterization of the test rig coupled to the REmSA prototype. The considered MF method is then tested to evaluate its performance in a realistic setup.

A. TEST BENCH CHARACTERIZATION

An experimental plant characterization is performed in the frequency domain to verify the validity of the numerical

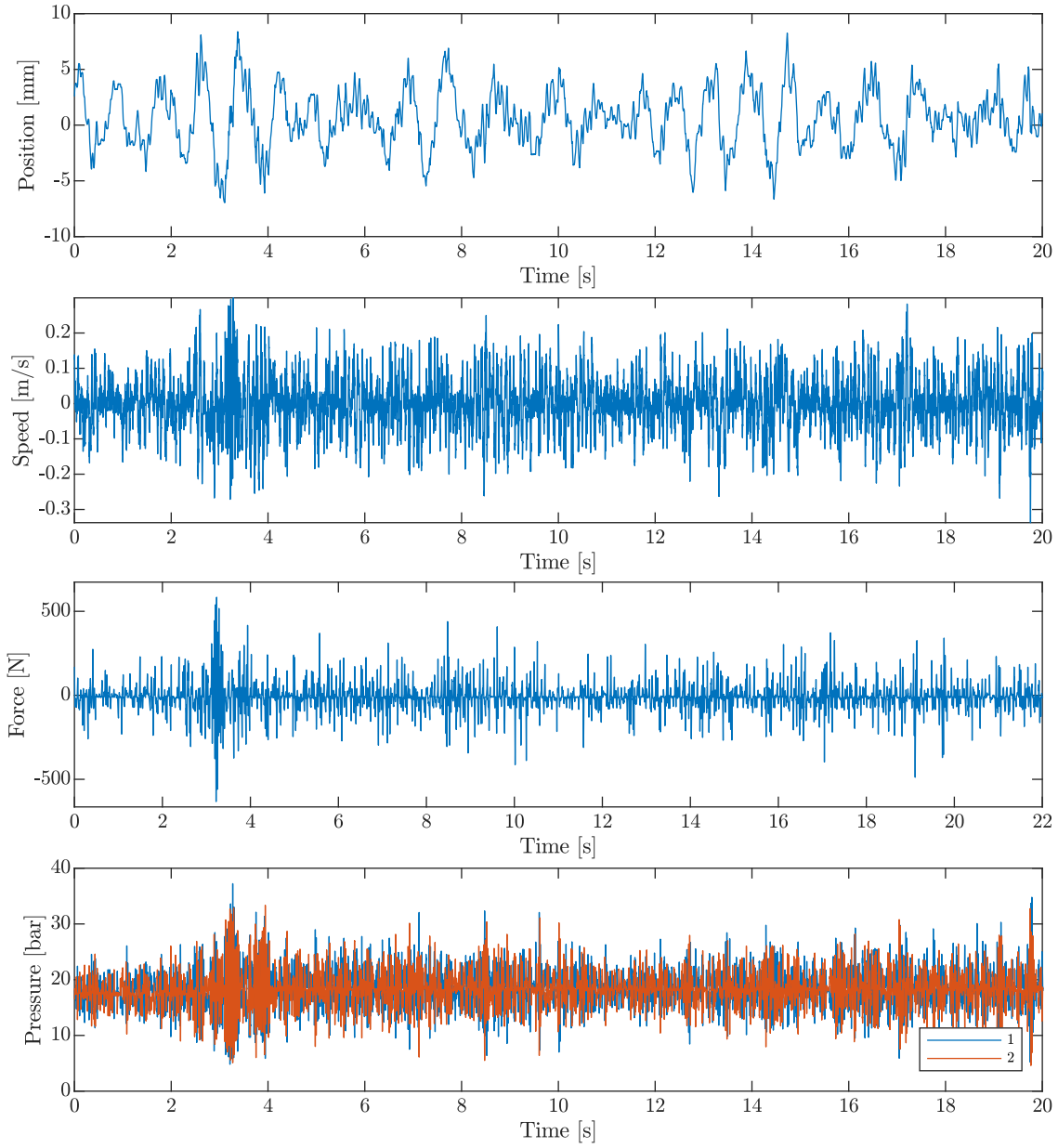

FIGURE 10. Hardware-in-the-loop experiment. Hydraulic piston position, speed, force, and line pressure measurements with null damping imposed, while simulating a quarter car model traveling at 70 km/h on a ISO-B road profile.

model. Specifically, the null-damping setup is considered. A sinusoidal sweep signal with a constant amplitude $|\theta_{l,ref}| = 0.5$ deg is set through frequencies between 1 and 30 Hz. The frequency response function (FRF) of the testbed is obtained as the ratio between output and reference signal fast Fourier transforms (Fig. 9). The FRF shows a resonant peak at 17 Hz, which is comparable to the 15 Hz obtained in the closed-loop model of Fig. 5 without compensation (yellow line). This behavior is followed by subsequent attenuation, as expected. The discrepancy between the resonant peaks is explained by the increase in oil temperature during the sine sweep test. This phenomenon causes a reduction of the oil viscosity, leading to a stiffer and less damped circuit. Consequently, the experimental resonant peak appears at a slightly higher frequency and with a higher magnitude. Moreover, a trend towards a unitary module (0 dB) is observed as the frequency approaches zero.

B. TEST WITH NULL DAMPING

Test bench results obtained without electromagnetic damping contributions from the prototype are plotted in Fig. 10, considering an ISO-B input road profile and a vehicle speed of 70 km/h. They contain relevant signals from the test bench sensors: position and speed from the stroke sensor inside the hydraulic actuator, piston force measurements from the

load cell, and pressure signal from both lines of the hydraulic circuit.

The tracking performance of the test rig is evaluated by comparing the angular rotation reference coming from the quarter car model in real time with the acquired displacement obtained through the position transducer installed inside the hydraulic piston. The testbed driving motor current is saturated to a maximum value of 70 A. When this saturation is reached, chattering due to saturation may appear. This can be observed as brief but strong oscillations in the force and pressure signals of Fig. 10. Careful tuning of the position control can attenuate this effect.

To validate tracking performance in this test at null damping, Fig. 11 compares the measured lever position with its reference. In this case, experimental angle signal tracking yields $g = 84.7\%$.

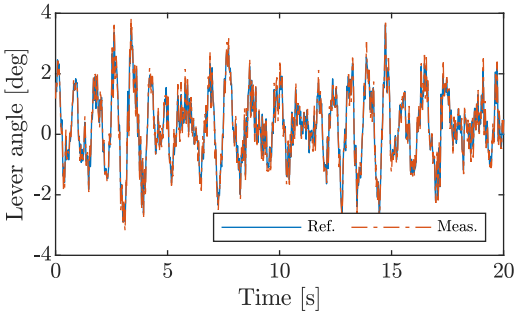

FIGURE 11. Hardware-in-the-loop experiment. Lever angle tracking with null damping imposed, while simulating a quarter car model traveling at 70 km/h on a ISO-B road profile.

Figure 12 reports voltage, current and power on the DC-link battery of the REmSA during this null-damping test. Positive power values flow from the battery to the actuator.

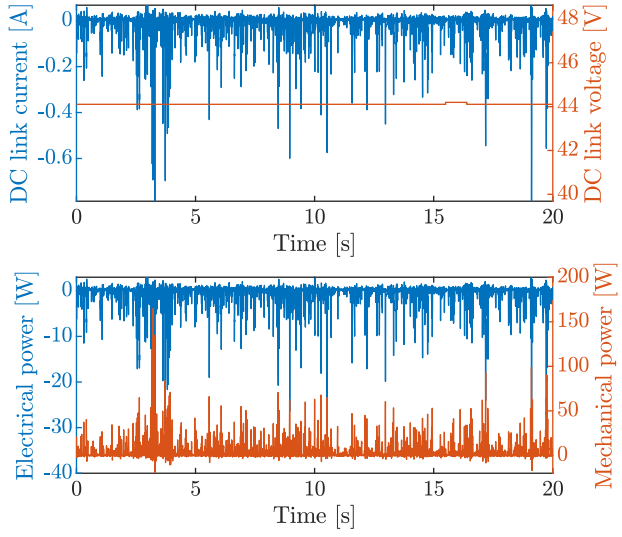

FIGURE 12. Hardware-in-the-loop experiment. DC-link voltage, current, power, and mechanical power with null damping imposed, while simulating a quarter car model traveling at 70 km/h on a ISO-B road profile.

For comparison purposes, the mechanical power applied by the test bench is also plotted. Likewise, positive power flows from the testbed to the actuator. Thus, predominantly positive mechanical power demonstrates that the REmSA is working as a damper, with an average power of 4.09 W. It is noted that this power dissipation takes place in the mechanical domain, as the battery does not experience this power flow interaction, due to the fact that $c_{\text{em}} = 0$. Hence, very little regeneration takes place, and an average DC-link power of -0.62 W is obtained.

C. TESTS WITH THREE DAMPING VALUES

Provided the positive tracking performance in III-B, a model mismatch between the compensation scheme and the test rig is introduced to validate the method against parametric uncertainty on the load. Figure 13 depicts the results obtained by applying an electromagnetic damping value c_{em}

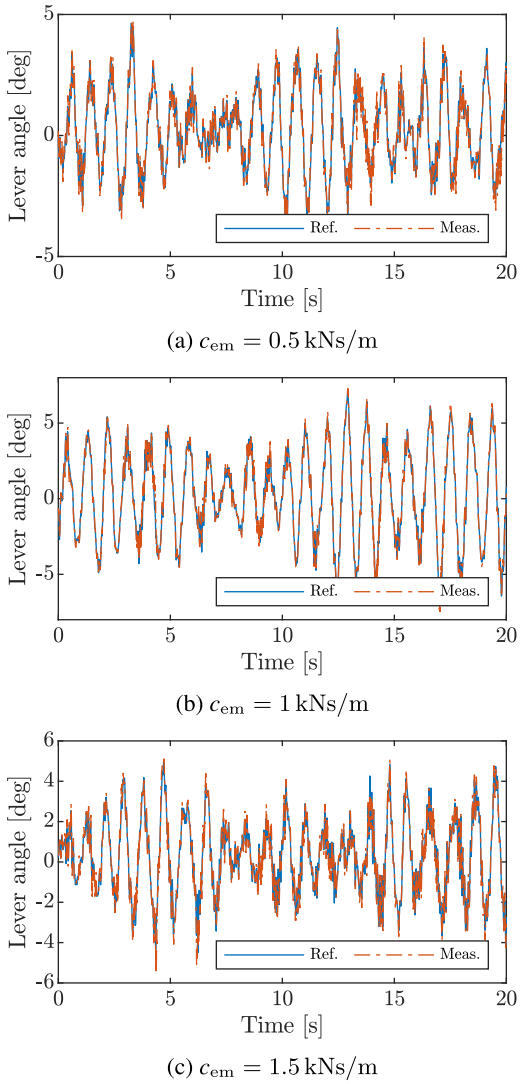

FIGURE 13. Hardware-in-the-loop experiment. Lever angle tracking with 0.5, 1, and 1.5 kNs/m of damping imposed, while simulating a quarter car model traveling at 70 km/h on a ISO-B road profile.

of 0.5, 1, and 1.5 kNs/m to the REmSA prototype, while applying an ISO-B input road profile and a vehicle speed of 70 km/h. No changes to the formulation of the compensation scheme are provided, i.e. the method is tuned assuming $c_{\text{em}} = 0$.

Table 1 lists the g ratios and the RMS current of the input motor during the three experiments. This latter term is a key indicator of the method stability during the tests, as an elevated command activity usually implies chattering and actuator saturation. It is seen that the RMS current gradually increases for ascending damping values; the test bench in HiL configuration with model mismatch leads to an increased number of oscillating points during the test, hence saturating locally the current absorbed and increasing the resulting RMS value. However, lever position tracking is favorable ($g > 82\%$), even in the presence of the worst parameter mismatch ($c_{\text{em}} = 1.5$ kNs/m). The results in Fig. 13 provide proper tracking of the lever angle in all the damping conditions, even when the actuator shows limitations due to intrinsic saturation and consequent command chattering. Figure 14 illustrates the command activity in terms of current of the input motor. Multiple instances where the command reaches saturation and oscillates are observed.

TABLE 1. Performance metrics of the controlled testbed for different electromagnetic damping settings.

REmSA damping [kNs/m]	Input motor RMS current [A]	g [%]
0	11.12	84.7
0.5	19.07	83.1
1	21.07	87.6
1.5	21.66	82.4

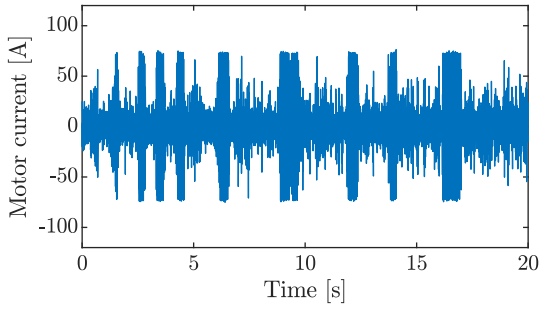

FIGURE 14. Hardware-in-the-loop experiment. Input motor current with 1.5 kNs/m of damping imposed, while simulating a quarter car model traveling at 70 km/h on a ISO-B road profile.

IV. CONCLUSION

The present paper described a hardware-in-the-loop approach for evaluating active shock absorbers. Specifically, an electromechanical rotary electromagnetic shock absorber was tested with an electro-hydrostatic test bench reproducing real working conditions computed through a quarter car model in real time.

Due to instability issues arising from the interaction of the unsprung mass and the test bench natural frequencies, a compensation method was required for implementing HiL. From simulation on the entire testbed model, the model following approach resulted as the most suitable one to enhance the actuation bandwidth of the test rig

Simulations on a ISO-B at 70 km/h showed a favorable reference tracking of the prototype model. Then, the compensation method was tested on a physical test bench, showing successful tracking and reliability during HiL. The test rig was tested with parametric variations of the electromagnetic damping, which changes the load of the active suspension. Chattering phenomena were observed due to the intrinsic limitations of the input motor. However, the tracking kept stable even in the presence of these effects.

Further developments of this research are the implementation of an adaptive model following to take into account variations of the required damping at vehicle level. Additionally, the validity of the method can be tested while applying active suspension control strategies on the load.

APPENDIX A
TEST BENCH PARAMETERS

Description	Symbol	Value
Motor torque constant	K_{in}	3 Nm/A
Motor saturation current	$i_{\text{in}}^{\text{sat}}$	70 A
Motor-pump inertia	J_θ	0.1 kgm^2
Pump viscous damping	c_θ	0.3 Nms/rad
Pump displacement	D_{p}	$1.81 \cdot 10^{-6}$ m^3/rad
Piston area	A_{p}	$1.05 \cdot 10^{-4}$ m^2
Fluid viscous damping	c_{h}	$8 \cdot 10^{10}$ Ns/m^5
Fluid stiffness	k_{h}	$1.695 \cdot 10^{13}$ N/m^5
Piston mass	m_{p}	12.76 kg
Piston viscous damping	c_{p}	1 kNs/m

APPENDIX B
ROTARY ELECTROMAGNETIC SHOCK ABSORBER AND QUARTER CAR PARAMETERS

Description	Symbol	Value
Transmission lever length	l_{r}	0.115 m
Gearbox transmission ratio	τ_{r}	1/87.35
REmSA motor torque constant	K_{r}	0.0493 Nm/A
Sprung mass	m_{s}	416.5 kg
Unsprung mass	m_{u}	40 kg
Spring stiffness	k_{s}	23.26 kN/m
Tire stiffness	k_{u}	223 kN/m
Passive damping	c_{s}	0
Tire damping	c_{u}	0
REmSA eq. mass	m_{eq}	5.58 kg
REmSA eq. viscous damping	c_{eq}	200 Ns/m
Road grade coefficient	G_{r}	$6.4 \cdot 10^{-7}$ m $\cdot$ cycle
Vehicle longitudinal speed	v_{car}	19.44 m/s
Road cut-off frequency	ω_0	1.22 rad/s

APPENDIX C
TEST BENCH POSITION CONTROL PARAMETERS

Description	Symbol	Value
Proportional gain	P	3
Integral gain	I	0.1
Derivative gain	D	0.03
Filter coefficient	N	600
Sample time	T_{s}	0.25 ms

APPENDIX D
TRANSFER FUNCTION COEFFICIENTS

Symbol	Value	Symbol	Value
k_1	$2.145 \cdot 10^9$	p_3	8516
k_2	$2.145 \cdot 10^{14}$	p_4	613
k_3	99341	a_1	114.9
z_1	211.9	a_2	$1.082 \cdot 10^4$
p_1	11.3	a_3	6579
p_2	$6.283 \cdot 10^4$	a_4	$4.082 \cdot 10^7$

ACKNOWLEDGMENT
The authors would like to thank the staff at Marelli Ride Dynamics for their valuable support throughout this research activity.

REFERENCES
[1] D. Fischer and R. Isermann, "Mechatronic semi-active and active vehicle suspensions," *Control Eng. Pract.*, vol. 12, no. 11, pp. 1353–1367, Nov. 2004.
[2] J. Yang, D. Ning, S. S. Sun, J. Zheng, H. Lu, M. Nakano, S. Zhang, H. Du, and W. H. Li, "A semi-active suspension using a magnetorheological damper with nonlinear negative-stiffness component," *Mech. Syst. Signal Process.*, vol. 147, Jan. 2021, Art. no. 107071.
[3] Y. Huang, Y. Sun, J. Ding, S. Yuan, J. Zhao, M. Wang, J. Luo, and H. Pu, "Design and analysis of a stiffness and damping regulator based on giant electrorheological fluid under multilayered squeeze mode," *J. Sound Vibrat.*, vol. 527, Jun. 2022, Art. no. 116864.
[4] H. Zhao, B. Wang, and G. Chen, "Numerical study on a rotational hydraulic damper with variable damping coefficient," *Sci. Rep.*, vol. 11, no. 1, p. 22515, Nov. 2021.
[5] L. Zuo and P.-S. Zhang, "Energy harvesting, ride comfort, and road handling of regenerative vehicle suspensions," *J. Vibrat. Acoust.*, vol. 135, no. 1, pp. 295–302, Feb. 2013.
[6] B. L. J. Gysen, T. P. J. van der Sande, J. J. H. Paulides, and E. A. Lomonova, "Efficiency of a regenerative direct-drive electromagnetic active suspension," *IEEE Trans. Veh. Technol.*, vol. 60, no. 4, pp. 1384–1393, May 2011.
[7] R. Galluzzi, Y. Xu, N. Amati, and A. Tonoli, "Optimized design and characterization of motor-pump unit for energy-regenerative shock absorbers," *Appl. Energy*, vol. 210, pp. 16–27, Jan. 2018.
[8] R. Galluzzi, S. Circosta, N. Amati, and A. Tonoli, "Rotary regenerative shock absorbers for automotive suspensions," *Mechatronics*, vol. 77, Aug. 2021, Art. no. 102580.
[9] M. A. A. Abdelkareem, L. Xu, M. K. A. Ali, A. Elagouz, J. Mi, S. Guo, Y. Liu, and L. Zuo, "Vibration energy harvesting in automotive suspension system: A detailed review," *Appl. Energy*, vol. 229, pp. 672–699, Nov. 2018.
[10] R. Galluzzi, S. Circosta, N. Amati, and A. Tonoli, "Performance comparison between electromechanical and electro-hydrostatic regenerative shock absorbers," *IOP Conf. Ser., Mater. Sci. Eng.*, vol. 1214, no. 1, Jan. 2022, Art. no. 012012.
[11] W. E. Misselhorn, N. J. Theron, and P. S. Els, "Investigation of hardware-in-the-loop for use in suspension development," *Vehicle Syst. Dyn.*, vol. 44, no. 1, pp. 65–81, Jan. 2006.
[12] D. C. Batterbee and N. D. Sims, "Hardware-in-the-loop simulation of magnetorheological dampers for vehicle suspension systems," *Proc. Inst. Mech. Eng., I, J. Syst. Control Eng.*, vol. 221, no. 2, pp. 265–278, Mar. 2007.
[13] V. Beliautsou, J. Alfonso, J. Giltay, F. Büchner, B. Shyrokau, J. A. Castellanos, and V. Ivanov, "Validation of integrated EV chassis controller using a geographically distributed X-in-the-loop network," in *Proc. IEEE Vehicle Power Propuls. Conf. (VPPC)*, Nov. 2022, pp. 1–7.
[14] C. Lauwerys, J. Swevers, and P. Sas, "Robust linear control of an active suspension on a quarter car test-rig," *Control Eng. Pract.*, vol. 13, no. 5, pp. 577–586, May 2005.
[15] C. Sandu, E. R. Andersen, and S. Southward, "Multibody dynamics modelling and system identification of a quarter-car test rig with McPherson strut suspension," *Vehicle Syst. Dyn.*, vol. 49, nos. 1–2, pp. 153–179, Feb. 2011.
[16] M. Yu, C. Arana, S. A. Evangelou, D. Dini, and G. D. Cleaver, "Parallel active link suspension: A quarter-car experimental study," *IEEE/ASME Trans. Mechatronics*, vol. 23, no. 5, pp. 2066–2077, Oct. 2018.
[17] M. Yu, C. Arana, S. A. Evangelou, and D. Dini, "Quarter-car experimental study for series active variable geometry suspension," *IEEE Trans. Control Syst. Technol.*, vol. 27, no. 2, pp. 743–759, Mar. 2019.
[18] Y. Taskin, Y. Hacioglu, and N. Yagiz, "Experimental evaluation of a fuzzy logic controller on a quarter car test rig," *J. Brazilian Soc. Mech. Sci. Eng.*, vol. 39, no. 7, pp. 2433–2445, Jul. 2017.
[19] S. Hashemi, M. Montazeri, and M. Nasiri, "The compensation of actuator delay for hardware-in-the-loop simulation of a jet engine fuel control unit," *Simulation*, vol. 90, no. 6, pp. 745–755, Jun. 2014.
[20] C. Chen and J. M. Ricles, "Analysis of actuator delay compensation methods for real-time testing," *Eng. Struct.*, vol. 31, no. 11, pp. 2643–2655, Nov. 2009.
[21] A. Tonoli, N. Amati, J. G. Detoni, R. Galluzzi, and E. Gasparin, "Modelling and validation of electromechanical shock absorbers," *Vehicle Syst. Dyn.*, vol. 51, no. 8, pp. 1186–1199, Aug. 2013.
[22] M. Guiggiani, *The Science of Vehicle Dynamics: Handling, Braking, and Ride of Road and Race Cars*. Cham, Switzerland: Springer, 2023.
[23] C. Liu, L. Chen, H. P. Lee, Y. Yang, and X. Zhang, "Generalized skyhook-groundhook hybrid strategy and control on vehicle suspension," *IEEE Trans. Veh. Technol.*, vol. 72, no. 2, pp. 1689–1700, Feb. 2023.
[24] T. T. H. Tran, T. A. Nguyen, T. B. Hoang, D. N. Nguyen, and N. D. Dang, "Optimizing the parameter of the lqr controller for active suspension system," in *Proc. Regional Conf. Mech. Manuf. Eng.* Cham, Switzerland: Springer, 2021, pp. 260–270.
[25] M. Yu, S. A. Evangelou, and D. Dini, "Parallel active link suspension: Full car application with frequency-dependent multiobjective control strategies," *IEEE Trans. Control Syst. Technol.*, vol. 30, no. 5, pp. 2046–2061, Sep. 2022.
[26] *Mechanical Vibration Road Surface Profiles Reporting of Measured Data*, document ISO, ISO 8608, International Organization for Standardization, 2016.
[27] D. Xinmin, X. Zhiguo, and L. Qin, "Gain scheduled model following control of flight control system based on neural network," in *Proc. Int. Conf. Neural Netw. Signal Process.*, 2003, pp. 301–305.
[28] D. Wang, Z. Wang, S. Wu, and S. Okubo, "Model following control system with robot system," in *Proc. 2nd Int. Asia Conf. Informat. Control, Autom. Robot. (CAR)*, vol. 2, Mar. 2010, pp. 445–448.
[29] C. Chen and J. M. Ricles, "Improving the inverse compensation method for real-time hybrid simulation through a dual compensation scheme," *Earthq. Eng. Struct. Dyn.*, vol. 38, no. 10, pp. 1237–1255, Aug. 2009.

MANFREDI TORNABENE received the M.Sc. degree in automotive engineering from Politecnico di Torino, Italy, in July 2021, where he is currently pursuing the Ph.D. degree in mechanical engineering. His research interests include design, control and validation of mechatronic suspension systems for ground vehicles.

GENNARO SORRENTINO received the M.Sc. degree in automotive engineering from Politecnico di Torino, Italy, in December 2020, where he is currently pursuing the Ph.D. degree in mechanical engineering. His research interests include the design, control, and validation of mechatronic devices for automotive applications, and their impact on vehicle dynamics.

RENATO GALLUZZI (Senior Member, IEEE) was born in Mexico City, Mexico, in 1986. He received the M.Sc. and Ph.D. degrees in mechatronics from Politecnico di Torino, Italy, in 2010 and 2014, respectively. Since 2011, he has been an active collaborator with the Mechatronics Laboratory, Politecnico di Torino. He is currently a Research Professor with the School of Engineering and Sciences, Tecnológico de Monterrey, Mexico. He also holds inventorship in multiple international patents. He is the author of numerous journal publications and conference papers. His research interests include vibration control and damping systems, power actuators, electric machinery, and energy harvesting.

ANDREA TONOLI received the Ph.D. degree in machine design from Politecnico di Torino, Turin, Italy, in 1993. In 1994, he joined Politecnico di Torino, as a Faculty Member. From 2007 to 2011, he was the Director of the Mechatronics Laboratory, Politecnico di Torino. He is currently a Full Professor with the Department of Mechanical and Aerospace Engineering, Politecnico di Torino. His research interests include the analysis, design, and control of electromechanical systems, with an emphasis on rotating machinery, active and passive magnetic bearings and dampers, piezoelectric transducers for vibration and motion control, and electromechanical systems for automotive applications.

NICOLA AMATI received the Ph.D. degree in machine design from the Department of Mechanical Engineering, Politecnico di Torino, Turin, Italy, in 2001. In 2001, he joined the Politecnico di Torino, as a Faculty Member, where he is currently a Full Professor with the Department of Mechanical and Aerospace Engineering and a Coordinator of the Center for Automotive Research and Sustainable Mobility@PoliTO (CARS). His research and teaching interests include the analysis, design, and control of electromechanical systems with an emphasis on rotating machinery, active and passive magnetic bearings and dampers, and more electric systems for automotive applications.